Annals of Glaciology 9 1987

A MULTI-SENSOR APPROACH TO THE INTERPRETATION OF RADAR ALTIMETER WAVE FORMS FROM TWO ARCTIC ICE CAPS

by

Mark R. Drinkwater and Julian A. Dowdeswell*

(Scott Polar Research Institute, University of Cambridge, Cambridge CB2 1ER, U.K.)

ABSTRACT

Data collected over Svalbard on 28 June 1984 by a 13.81 GHz airborne radar altimeter enabled analysis of signals returned from two relatively large ice masses. Wave forms received over the ice caps of Austfonna and Vestfonna are analysed with the aid of existing aerial photography, radio echo-sounding data, and Landsat MSS images acquired close to the date of the altimeter flight. Results indicate that altimeter wave forms are controlled mainly by surface roughness and scattering characteristics. Wet snow surfaces have narrow 3 dB back-scatter half-angles and cause high-amplitude signals, in contrast to relatively dry snow surfaces with lower-amplitude diffuse signals. Metre-scale surface roughness primarily affects wave-form amplitude and leading-edge slope, this becoming apparent over ice streams on Vestfonna.

INTRODUCTION

The European Space Agency's ERS-1 satellite will carry a suite of Earth remote-sensing instruments on a dedicated polar and oceanographic mission. For studies of large ice masses, an important component of its payload will be a Ku-band radar altimeter with the capability of providing precise surface elevations of Arctic and Antarctic ice masses (cf. Zwally and others 1983). It will yield synoptic information on the topography of major ice-sheet and ice-cap surfaces, enabling morphological and mass-balance studies to be undertaken. In addition to the radar altimeter's capability of returning accurate range data, however, it also returns information in the record of energy back-scattered from the surface. Few investigations have been made of the resulting wave forms, and their relationship to ice-mass surface character.

The aims of this paper are, first to analyse the nature of radar altimeter wave forms received from two Arctic ice caps and, secondly, to interpret these data with the aid of other information on ice-mass elevations and characteristics of the ice surface. Data were collected during the 1984 Marginal Ice Zone Experiment on 28 June 1984 using an aircraft-mounted 13.81 GHz radar altimeter, designed and constructed by the Rutherford Appleton Laboratory (RAL) (McIntyre and others 1986). This provided an opportunity to examine wave forms obtained over relatively large terrestrial ice masses.

Some 400 track kilometres of radar-altimetric data were acquired over the ice caps of Austfonna (8105 km^2) and Vestfonna (2510 km^2) in Nordaustlandet, Svalbard (Fig.1). Three sections of the altimetric data are analysed in detail to illustrate a number of points concerning ice-surface characteristics and topography. Information from other sensors is also used to aid interpretation of the altimeter wave forms. Ice-surface topographic data from airborne radio echo-sounding (RES) of the ice caps are available (Dowdeswell and others 1986), and the character of the ice surface has also been investigated using a combination of aerial photographs and Landsat images acquired close to the date of the flight.

*Present address: Department of Geography, University College of Wales, Aberystwyth, Penglais, Aberystwyth, Dyfed SY23 3DB, UK.

BACKGROUND: SCATTERING FROM SNOW AND ICE AT NEAR-NORMAL INCIDENCE

The main factors influencing scattering of radar pulses from snow and ice surfaces are outlined prior to analysis and interpretation of altimetric data from the Nordaustlandet ice caps. Moore and Williams (1957) suggested that the mean pulse returns received by an altimeter correspond mainly to incoherent back-scattering from a rough surface. If volume scattering is considered negligible, a model mean pulse return may be expressed as a convolution of two parts: the transmitted pulse shape and a function including the antenna-beam pattern, ground properties, and range to target. Brown (1977) incorporated and refined these ideas in a model of rough-surface scattering by including an explicit expression for the antenna pattern and variation of back-scatter with angle.

Passive microwave radiometric data were obtained during the same flight by imaging and non-imaging instruments operating at wavelengths from 0.3 to 1.7 cm. Gloersen and others (1985) concluded from brightness temperatures recorded that the surface layer was close to melting point throughout most of Nordaustlandet. Many areas will therefore have had a relatively high volumetric free-water content in the surface layers. The resulting dielectric discontinuity between the air and snow is large, preventing significant penetration of pulses. From this, we may deduce that scattering of the transmitted altimeter pulses occurs almost exclusively at the surface over Nordaustlandet. Even when snow is dry, back-scatter at nadir will be dominated by surface scattering, using typical values for snow parameters taken from Ulaby and others (1982). This enables the use of a model incorporating rough-surface theory to understand variations in wave forms obtained in Nordaustlandet.

Ulander (unpublished) discussed the use of Brown's model in understanding mean pulse returns over planar ice sheets, with the proviso that its assumptions are only interpreted as first-order approximations of surface character. The main drawback of the model is that ice masses are variable across the altimeter footprint. A series of predicted mean RAL altimeter pulse shapes, which Ulander generated using Brown's model, is shown in Fig.2. This illustrates the effects of different values for RMS surface roughness (Fig.2a) and for the "surface polar-scattering diagram" or angular dependence of scattering (Fig.2b), which is quantified in terms of the 3 dB back-scatter half-angle (i.e. the angle from normal incidence to the point at which the back-scatter coefficient is reduced to half its maximum value, assuming a Gaussian back-scatter function and which is here abbreviated to TBH). Increasing RMS roughness at the metre-scale reduces peak power and increases rise time, and increasing back-scatter half-angle causes more diffuse returned signals with progressively longer durations. These idealized wave forms are presented for comparison with the data obtained from Nordaustlandet shown in the subsequent analysis.

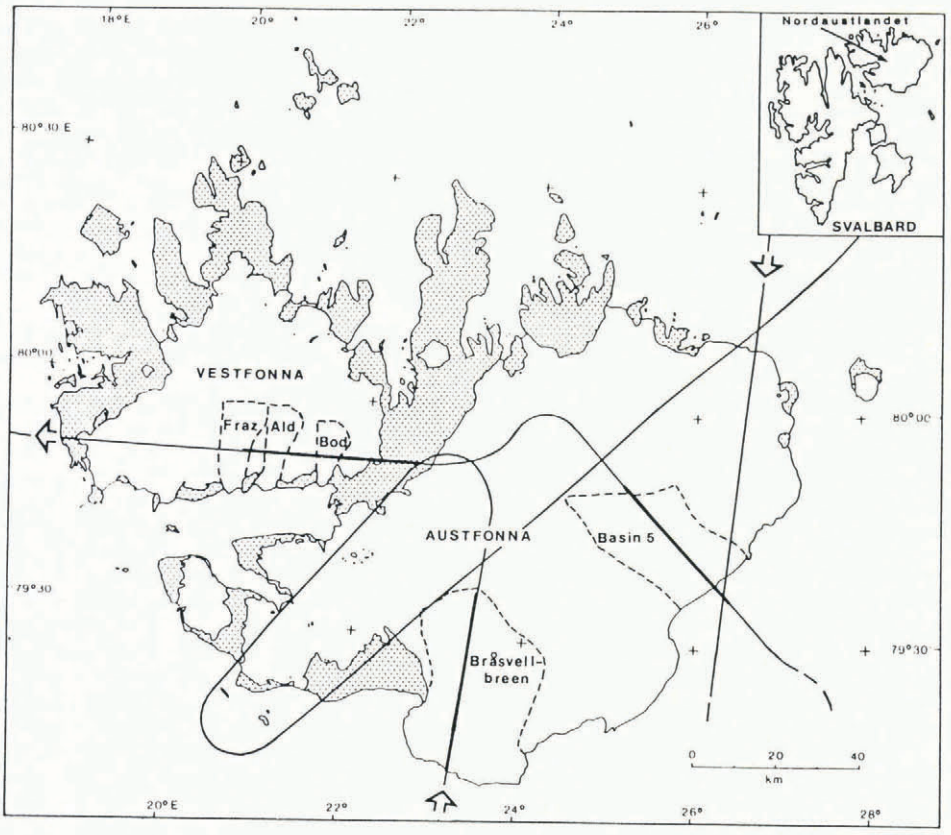

Fig.1. Map of Nordaustlandet ice caps illustrating the full radar-altimeter flight track and sections analysed in detail (heavy). The location of Nordaustlandet within Svalbard is inset.

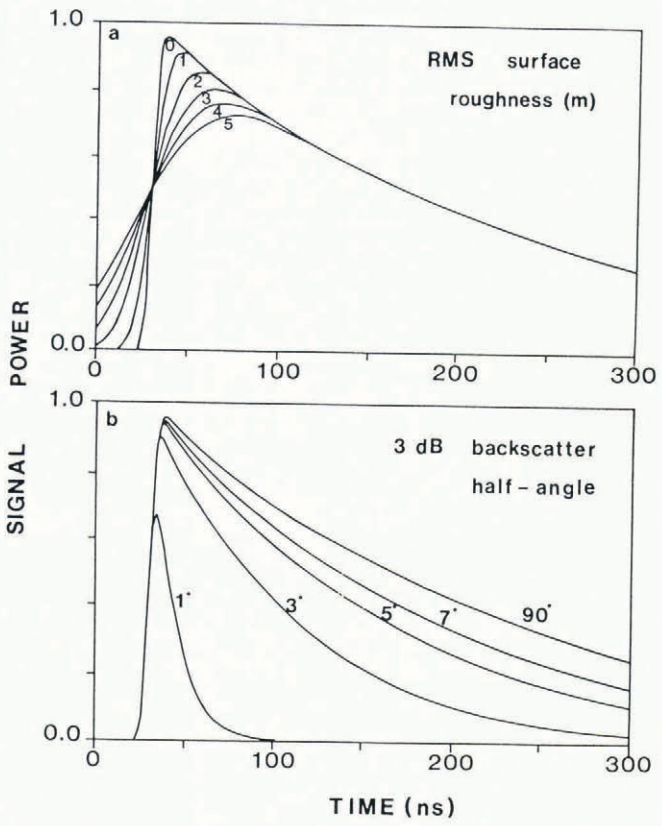

Fig.2. Predicted pulse shapes for variations in (a) surface roughness and (b) TBH, using a 7.3 ns pulse duration. All have been normalized assuming constant back-scatter coefficient at normal incidence and antenna gain, and Gaussian variation of back-scatter coefficient with angle (adapted from Ulander unpublished).

Various approaches to modelling have demonstrated that for comparatively rough surfaces, such as glacier ice, the coefficient of back-scatter becomes independent of radar frequency and depends on surface RMS slope, reflectivity, and incidence angle (Ulaby and others 1982). For locally smooth surfaces with only gentle undulations, such as snow surfaces, surface scattering may be separated into a coherent (specular) component, and a non-coherent (diffuse) component (Fung 1981).

Properties affecting scattering include:

i. Water content;
ii. Surface roughness;
iii. Reflectivity;
iv. Crystal structure;
v. Density of snow-pack.

The presence of small amounts of free water in snow is known to affect the loss tangent of the snow significantly. For example, a free-water content of 1% by weight will increase the loss tangent from 0.001 to 0.01 in dry snow (Cumming 1952), thereby substantially reducing signal penetration. The penetration depth through snow is reduced to about one wavelength for free-water contents of only 3–4% by volume. Temperature variations also influence snow-crystal metamorphism and alter the texture of the surface, thus affecting scattering. Reflectivity is determined by the permittivity of the medium and controls reflection from and transmission across the air/medium interface. Finally, the crystal structure and density of the medium are most likely to influence the directionality and strength of scattered energy. Intuitively, because of differences in material properties between wet snow, dry snow, and bare ice, we may expect each to have different scattering signatures.

METHODS

Altimetric data collection and navigation

The RAL altimeter was mounted in a NASA CV-990 aircraft. Measurements were made with a nadir-pointing

https://doi.org/10.3189/S0260305500200773 Published online by Cambridge University Press

horn antenna between 07.34 and 08.30 h on 28 June 1984 from an altitude of 10 km. A full 3 dB beam width of 10° determined a pulse-limited footprint diameter of approximately 1.75 km. Flight lines were planned to follow tracks previously surveyed during an airborne RES campaign over Nordaustlandet (Dowdeswell and others 1986). Additional instruments aboard the CV-990 included a metric camera, providing overlapping vertical photographic coverage. However, cloud cover during the flight precluded its use.

Signals were recorded using a Biomation wave-form digitizer, in which one biomation amplitude unit of power (bau) equals 15.6 mV. Wave forms were digitized at delay intervals in range bins (or range gates), where one bin equals 3.33 ns. Subsequent use of the "bau" and "bin" units in the text considerably simplifies the discussion of data. A background d.c. voltage from the detector introduces an offset in mean wave forms, equal to 4 bau. Before data were interpreted this background level was subtracted. Over the ice sheet, signal amplitude varied considerably but the instrument had a fixed receiver gain. This had important implications, since at one extreme very strong returns saturated the receiver while, at the other, returns were not separable from background noise. Instrument calibration was also necessary for the calculation of back-scatter coefficients (Ulander unpublished). External calibrations to determine the instrument parameters were undertaken over retro-reflectors located on the Norwegian island of Andøya, and internal calibration was possible during the flight using the instrument's in-built "calibration mode".

The aircraft's flight path was recorded on magnetic tape by the Airborne Digital Data Acquisition System and was derived from the on-board Inertial Navigation System (INS). First, corrections were applied to original records of latitude and longitude to eradicate biases caused by drift of the gyros in the INS mechanism, and the cumulative error was linearly redistributed throughout the flight. Secondly, the flight line was re-positioned by fixing its output to the known locations of timed crossings on to the ice caps. Navigational data recorded throughout the flight were used to give an accurate flight line, which was superimposed on satellite images (Fig.3).

Supporting data sets

We selected Landsat 5 Multispectral Scanner (MSS) imagery from 24 June, and 12 and 17 July 1984, since these dates bracketed the altimetric data set and were the nearest days on which partially cloud-free digital scenes were available. Digitally enhanced Landsat sub-scenes corresponding to each flight section are shown in Fig.3. These images provide information on the surface character of the ice caps. Even where slopes are less than 1° or 2°, relatively small changes in ice-surface topography are indicated by differences in radiance (Dowdeswell and McIntyre 1986). Changing ice-surface characteristics, for example snow density, crystal size, and water content, will also affect radiance recorded by the MSS. Digital enhancement of these MSS data recorded on Computer Compatible Tapes (CCTs) therefore reveals considerable detail of the ice-cap surface (Fig.3). Aerial photographs taken of the ice caps in other years, and field seasons on the ice caps in May 1983 and May 1986, provide further background to the interpretation of altimeter wave forms. Airborne RES data, including both surface and bedrock elevations (Dowdeswell and others 1986), were also important in planning the CV-990 flight lines.

Wave-form tracking and averaging

Algorithms have been designed by Ulander (unpublished) which derive mean statistics from RAL altimeter wave forms. Such methods are akin to tracking and averaging routines used to sum and average raw individual pulses on previous altimetric missions (MacArthur 1978). They also act as a data quality check, and include sorting routines which guard against spurious data resulting from instrument malfunctions, and data which are invalid geophysically, becoming incorporated in the analysis. For an altimeter flying over a variable surface, such as a large ice mass, rapid changes in the form of scattered radar energy may be encountered due to variations in surface geometry and material properties. There is a temptation, therefore, to decrease the number of wave forms averaged in order to minimize the surface area sampled. However, confidence in the mean statistical values is determined by sample size. The control which this has on confidence limits, and the corresponding integration times and along-track integration distances, are presented in Table I.

The statistics in Table I are calculated assuming a constant aircraft velocity of 200 m s^{-1} and a known pulse-repetition frequency of 100 Hz. However, with an unstable moving platform such as an aircraft, these integration distances may only be used as an approximate guide, since the effects of pitch and variable velocity either compress or extend along-track integration distance. Rejecting pulse wave forms during the sorting procedure also extends the sampling interval. For a sample size of 50, the integration distance has been observed to expand, at worst, by 100 m. Normally, the use of 100 pulses is statistically adequate to construct a mean wave form. However, for surfaces of high spatial variability, we may have to accept increased variance, due to inadequate averaging out of "fading" effects (Ulaby and others 1982), in order that the terrain characteristics do not change significantly during along-track averaging. Thus, for a mean wave form composed of typically 50 individual pulse wave forms, the 95% confidence limits on the mean power ($\overline{P}$) lie between $0.77\overline{P}$ and $1.35\overline{P}$. This corresponds to a range of approximately 2.5 dB. Such uncertainty in a single estimate of mean power, for example, must be taken into account when contiguous mean pulse wave forms are compared or geophysical parameters are extracted. The 2.5 dB range, although large, may still enable us to distinguish between: (a) bare ice and dry snow, which have a possible relative difference in Fresnel reflection coefficient of up to 7 dB, and (b) wet snow and dry snow, which have a possible relative difference of up to 11 dB in reflection coefficient (Evans 1965, Smith and Evans 1972).

Wave-form descriptors

Several parameters are extracted to describe mean pulse wave forms, and have been adapted from Ulander (unpublished):

TABLE I. CONFIDENCE LIMITS FOR POWER VALUES (P) OF MEAN WAVE FORMS CONSTRUCTED USING VARYING SAMPLE SIZES. CORRESPONDING INTEGRATION DISTANCES AND TIMES ARE INCLUDED

N	Integration distance m	Integration time s	95% Confidence limits for 2N degrees of freedom
10	40	0.2	$0.59\overline{P} <$ mean $< 2.10\overline{P}$
20	80	0.4	$0.67\overline{P} <$ mean $< 1.64\overline{P}$
50	200	1.0	$0.77\overline{P} <$ mean $< 1.35\overline{P}$
100	400	2.0	$0.81\overline{P} <$ mean $< 1.20\overline{P}$

https://doi.org/10.3189/S0260305500200773 Published online by Cambridge University Press

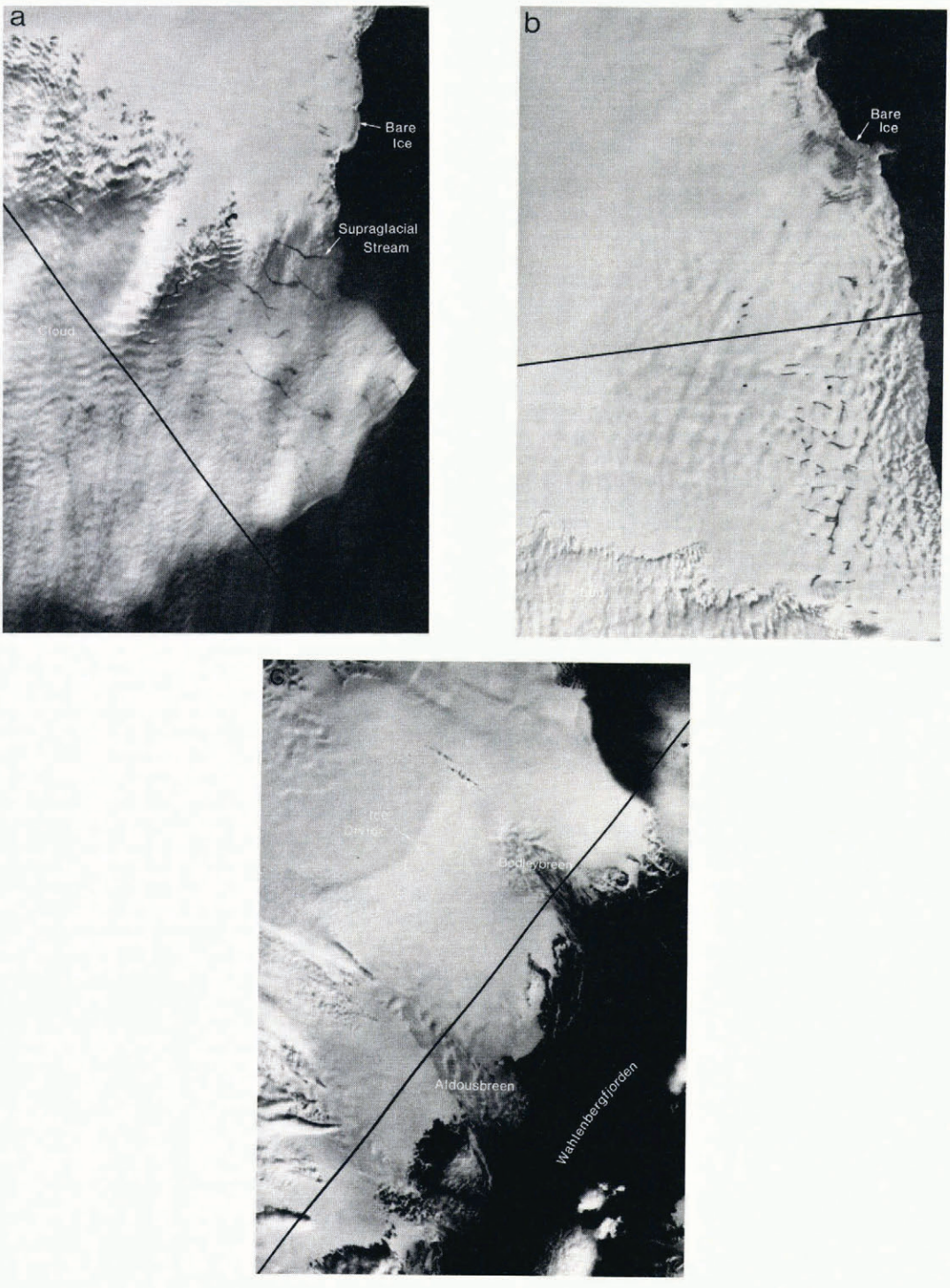

Fig.3. Digitally enhanced Landsat 5 images with the three flight tracks marked. Each image measures 28 km by 41 km.
(a) Brâsvellbreen on 12 July 1984 (Landsat path/row 214/03);

(b) Basin 5, Austfonna, on 17 July 1984 (217/02);

(c) Vestfonna on 24 June 1984 (216/02).

(1) Leading-edge slope (L_e). This is calculated by fitting a function to five points around the half-peak power point in a least-squares manner. It is expressed in dB bin^{-1} (where one range bin equals 3.33 ns).

(2) Calibrated coefficients of back-scatter (σ°). Each of the two coefficients expresses the gain (in dB) of an average scatterer on the ice-mass surface, assuming that the system point-target response is Gaussian with time.

(a) In the first algorithm the back-scatter coefficient (σ°_p) is calculated using the peak power of the received signal. This gives a measure of back-scatter at normal incidence (i.e. from within the first few range bins of the footprint). Since peak value is, in most cases, attained within the first few bins of the wave form, it is independent of the polar-scattering diagram of the surface. On the other hand, this value is sensitive to saturation effects in high-amplitude returns.

https://doi.org/10.3189/S0260305500200773 Published online by Cambridge University Press

(b) An alternative algorithm calculates a weighted value of the coefficient of back-scatter (σ_i°). This method assumes a "diffuse" return and so utilizes the sum or integral of power in the range bins occupied by the returned wave form. It is weighted to account for the antenna-beam attenuation pattern.

Accurate calculation of the coefficient of back-scatter necessitates that the aircraft tilt relative to the surface is small. A pitch, for example, of 1.5° would reduce back-scatter by about 0.5 dB, and so only flight sections where pitch and roll and regional slope are small (<1.5°) at all times were analysed.

(3) Trailing-edge attenuation coefficients (X). Since both coefficients of back-scatter are sensitive to pointing errors and surface-slope variations, and because they do not take into account variation in back-scatter with incidence angle, Ulander (unpublished) also used two trailing-edge attenuation coefficients to measure rates of decay in mean wave forms. They are applicable to wave forms with longer delays where power values are limited by antenna-beam attenuation.

(a) The early trailing-edge attenuation coefficient (X_e) is used to measure attenuation of power in the interval between 6 and 25 range bins after the wave-form peak. If we assume that signal power falls exponentially, then the following equation is used to calculate the coefficient of exponential decay:

$$y = ae^{-x} \qquad (1)$$

where y is power in units of bau, x is the coefficient of attenuation X_e, and a is a constant (300), scaling X_e to units of μs^{-1}.

(b) A late trailing-edge coefficient (X_1) is calculated in a similar manner for the interval 50 to 89 range bins after the wave-form peak.

The early trailing-edge attenuation coefficient gives good differentiation between mean returns of short duration, while the late attenuation coefficient gives better separation of longer-duration pulse returns. They are chosen to distinguish between surfaces having small 3 dB half-angles (i.e. 1–3°), and surfaces having large 3 dB half-angles (i.e. >3°). The latter coefficient is also independent of surface-height distribution effects on the received signals.

The above parameters are calculated for three sections of the altimeter flight over Austfonna and Vestfonna.

VARIATIONS IN WAVE-FORM PARAMETERS: BRÅSVELLBREEN, AUSTFONNA

Results

Mean wave forms from a long profile of Bråsvellbreen (Fig.1) are illustrated in Fig.4, with corresponding wave-form parameters in Fig.5. RMS surface roughness is also calculated from the standard deviation of pulse delays (Fig.5f). Fig.5a–g reveals three zones, after initial wave-form disruption caused by the inbound coastal crossing. Note that the boundaries between ice-surface zones discussed here are in reality transitional.

The first identifiable region lasts from approximately 3 to 17 km, and is characterized by the mean returns shown in Fig.4a and b. It is a period of relative stability and σ_p° and σ_i° show only slight steady increases, from 12 to 14 dB and 6 to 8 dB, respectively. X_e stays fairly constant at around 25 μs^{-1}, while an increase of X_1 from 2 to 10 μs^{-1} picks out the extended tails of wave-form trailing edges. Leading-edge gradient L_e (Fig.5c) fluctuates between 1.5 and 2.0 dB bin^{-1}, after having been stretched to 0.5 dB bin^{-1} at the 3 km stage. RMS surface roughness varies between 0.5 and 2.0 m (Fig.5f).

The second region lasts from 17 to 25 km, and is characterized by the mean wave forms in Fig.4c. Peak signal amplitudes reach their maximum, with σ_p° attaining a plateau at around 15 dB. Wave-form duration increases to 300 ns, resulting in a fall of X_e from 30 to 20 μs^{-1}.

The final region continues from 25 km until the end of the profile, and mean signals received at 31 km inland are displayed in Fig.4d. A marked reduction in signal amplitude occurs over the space of 5 km, and the coefficients of back-scatter σ_p° and σ_i° fall by 5 dB to 9 dB, and by 6 dB to 4 dB, respectively. Additionally, L_e (Fig.5c) falls to minima of below 1.0 dB bin^{-1}. More important, however, is the change occurring at around 29 km inland, after which both trailing-edge attenuation coefficients become markedly more variable. Beyond 35 km inland, signal amplitudes fall to their lowest values, and mean returns observed at 38 km

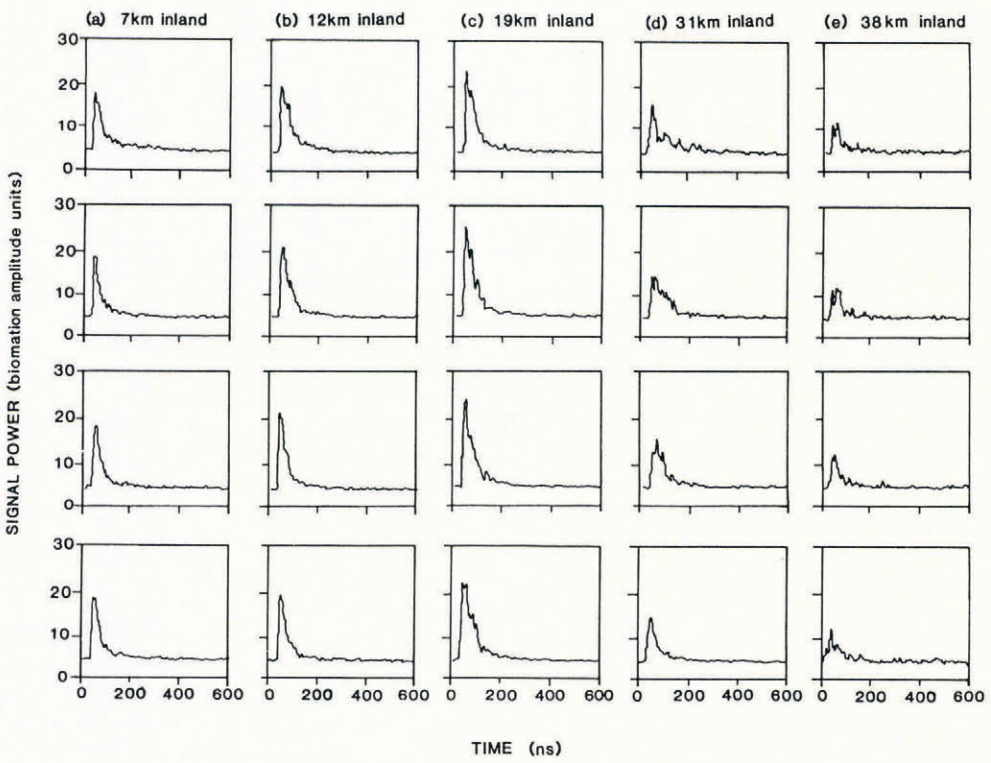

Fig.4. Four contiguous mean wave forms taken at five intervals along the Bråsvellbreen flight section (Fig.1) illustrating varying wave-form characteristics.

https://doi.org/10.3189/S0260305500200773 Published online by Cambridge University Press

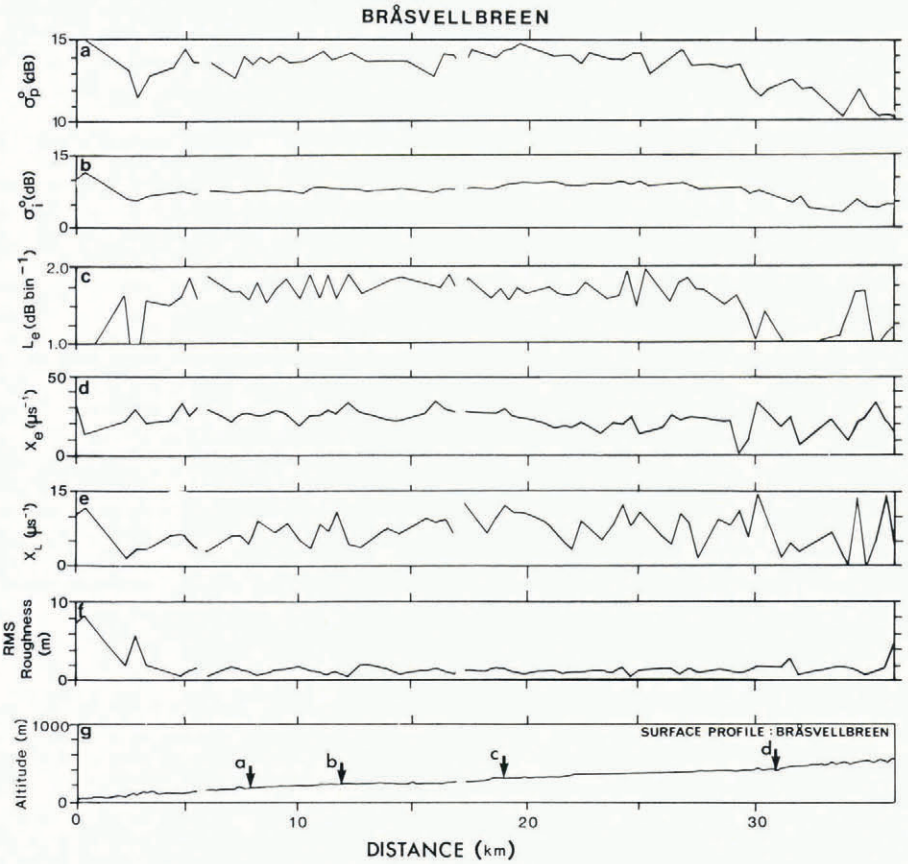

Fig.5 Traces of varying wave-form parameters and ice-surface profile along Bråsvellbreen flight section. The arrows labelled a to d in part g of the figure represent the locations of the sets of wave forms in Fig.4.

inland are displayed in Fig.4e. At this point the proportion of spurious delays increases, as many signals are too weak to be detected by the receiver. This situation is characteristic of the central parts of the ice cap.

Interpretation

Bråsvellbreen surged between 1936 and 1938, and is now in the quiescent period between surge activity (Schytt 1969). It has a regional gradient of less than 1°, and this minimizes inaccuracies in back-scatter calculations.

Comparison of the mean returns in Fig.4 with the model wave forms in Fig.2a and b indicates that over the sections identified progressive changes in wave-form geometry occur. Wave forms in Fig.4a, b, and c illustrate the increasing mean signal amplitudes and durations between 7 and 19 km. Throughout, signals have a specular component which dominates over a diffuse scattered component. As the bulk of each wave form is composed of reflected energy, they are termed "quasi-specular". Since signals do not principally result from diffuse scattering mechanisms, the two values of σ° (Fig.5a and b) show a consistent discrepancy, with σ°_p continually greater by 5 dB. Only in places where diffuse scattering becomes dominant will the two values meet and follow similar trends. Otherwise, although incorrect as an absolute value of σ°, the changes in σ°_i indicate variations in scatter contributions from angles off-nadir (Fig.5b). At this point, the surface has a narrow TBH, attaining a value of 3° at 19 km inland. Tonal variations on Landsat imagery indicate that most of the ice surface is snow-covered, apart from small coastal areas where bare ice is visible (Fig.3a). At this time of year the snow depth is likely to be significantly less than 1 m in depth within 25 km of the coast, and surface melting results in high free-water content in the upper layers. Snow depths are based on field surveys on Austfonna by Scott Polar Research Institute (SPRI) parties in spring 1983 and 1986. We suggest that in relatively wet snow areas the main mechanism causing near-specular signals is probably that of reflection from flat surfaces orientated perpendicular to incident pulses. Additional important effects are thought to be caused by reflections from supraglacial streams which cross the lower parts of the wet-snow zone. These streams are visible beneath thin cloud on the Landsat scene from 12 July (Fig.3a).

Maximum observed signal amplitudes occur between 17 and 25 km, and large TBH (over 3° in places) causes longer-duration wave forms (Fig.4c). More dense refrozen or glazed surface crusts, or shallow ice lamellae or lenses in this region (Schytt 1964), would explain the continuing dominance of the specular component of wave forms over the diffuse component.

From 25 km onwards signal amplitude falls considerably. This may be a response to moving to progressively higher elevations, where the effects of melting are reduced (Fig.4c). Surface melting and the formation of ice lenses has been observed even on the high crest of Austfonna (e.g. Schytt 1964, and SPRI party observations). However, whether or not surface melting had taken place high on Austfonna by late June 1984 is not certain. Trailing-edge attenuation remains fairly stable until 30 km, whereupon X_e and X_1 begin to fluctuate, in response to TBH varying between 3° and 7°. Variability in polar-scattering characteristics of dry snow surfaces has been observed by Ulander (unpublished). He derived a similar range of values from altimetry over central Greenland on 1 July. The cause of this variability is not understood, but it is most likely to be a combination of small-scale roughness and the reduced effects of snow-grain metamorphism.

In relatively dry snow some penetration may occur, and volume scattering is possible. However, at near-normal incidence surface scattering continues to dominate. If we assume a Gaussian height distribution, then the value of 1.5 dB bin^{-1} for L_e (Fig.5c) at 33 km corresponds with a value of 1 m surface roughness predicted by Brown's model for a similar leading-edge gradient. This matches our calculation of RMS surface roughness at 33 km (Fig.5f), and

https://doi.org/10.3189/S0260305500200773 Published online by Cambridge University Press

is similar to the height of wind-generated snow features such as sastrugi, dunes and ridges. Snow-feature dimensions observed by Ivanov (1968) range from a few centimetres to 2 m amplitude, with long axes from metres to several tens of metres. Beyond 30 km, peaks in RMS roughness are observed (Fig.5f), indicating larger-scale roughness than aeolian features (2 and 3 m). These account for some reduction in leading-edge gradient. Signals in Fig.4e have more rounded peaks and considerable variability in late bins.

VARIATIONS IN WAVE-FORM PARAMETERS: BASIN 5, AUSTFONNA

Results

Three zones are identifiable in this section of data; 0–7, 7–25, and 25–33 km (Fig.6). Between 0 and 7 km inland σ_p° is consistently the highest value of back-scatter by 10 dB (Fig.6a and b). L_e remains steady at 1.3 dB bin^{-1} (Fig.6c), but the attenuation coefficients fluctuate: X_e between 0 and 35 μs^{-1}, and X_1 between 0 and 15 μs^{-1}. The surface profile in Fig.6f has discontinuities indicating periods when the altimeter records spurious delays. These result from instrument malfunction or received signals being too weak to cross the triggering power threshold.

From 7 to 25 km, L_e becomes greater, attaining values comparable to those observed over Bråsvellbreen. There are increases in signal amplitude indicated by peaks in σ_p°, but σ_i° rises dramatically by over 10 dB in places following similar trends to σ_i°. In contrast, X_e falls to low values between 15 and 20 km, periodically reaching zero. X_1 attains values similar to those given over the section of several kilometres before the inbound coastal crossing indicated on the surface profile (Fig.6f).

In the final section (25 km onwards), parameters return to similar levels observed for the first 7 km over land. Once again, breaks in the profile indicate a large proportion of spurious altimeter delays.

Interpretation

Signals from 0 to 7 km are quasi-specular and comparisons made with Fig.2b yield a mean TBH of less than 3°. Despite the tall narrow peaks, however, some mean wave forms have shallower leading edges, resulting from large-scale surface roughness. The value of L_e of 1.2 dB bin^{-1} at 4 km inland corresponds with a surface-roughness prediction using Brown's model of the order of 3 m amplitude. Aerial photographs from previous field campaigns reveal that there is a high degree of crevassing and undulating serac ice in this coastal region and this would explain the loss or severe attenuation of many signals, and the resulting large number of spurious delays. However, the specular component of signals is likely to occur by reflections from wet snow and/or large planar ice surfaces between crevasses.

Aerial photography indicates that the surface is markedly less broken between 7 and 25 km inland despite large-scale surface perturbations of over 10 m height and several kilometres in wavelength. The profile in Fig.6f indicates that signals are strong in this part of the basin. The rise in σ_i° and similarity of the two back-scatter coefficients confirms that returns are diffuse, wave forms periodically having durations of over 300 ns and 3 dB half-angles between 5° and 7°.

It is useful at this point to make comparisons between diffuse land-ice signals and ocean returns, and the corresponding responses of the calculated wave-form parameters. Ocean returns (diffuse) are a useful yardstick since they result from Lambertian or isotropic surface scatter, tending to a 10° situation in Fig.2b (Gatley and Peckham 1983). Diffuse ocean returns characteristically exhibit high values of σ_p°, σ_i°, and X_1, with X_e returning zeros or very low values. By contrast, quasi-specular returns show high values for σ_p° and X_e with low σ_i° and X_1. Surface returns at 14 and 16 km show similar characteristics to ocean signals observed between −5 and 0 km, and L_e and X_1 return similar values, despite reduced back-scatter values. High-density snow with a refrozen crust or high water content is a known cause of high reflectances, while small-scale surface roughness is the suggested cause of wider polar scattering.

Between 20 and 25 km, mean signals return to values similar to those recorded in the initial 7 km over the ice cap, the TBH falling to around 3°. Scattering contributions are limited to highly reflective surfaces within the pulse-limited footprint, antenna-beam attenuation effectively suppressing weak returns from areas on the fringe of the

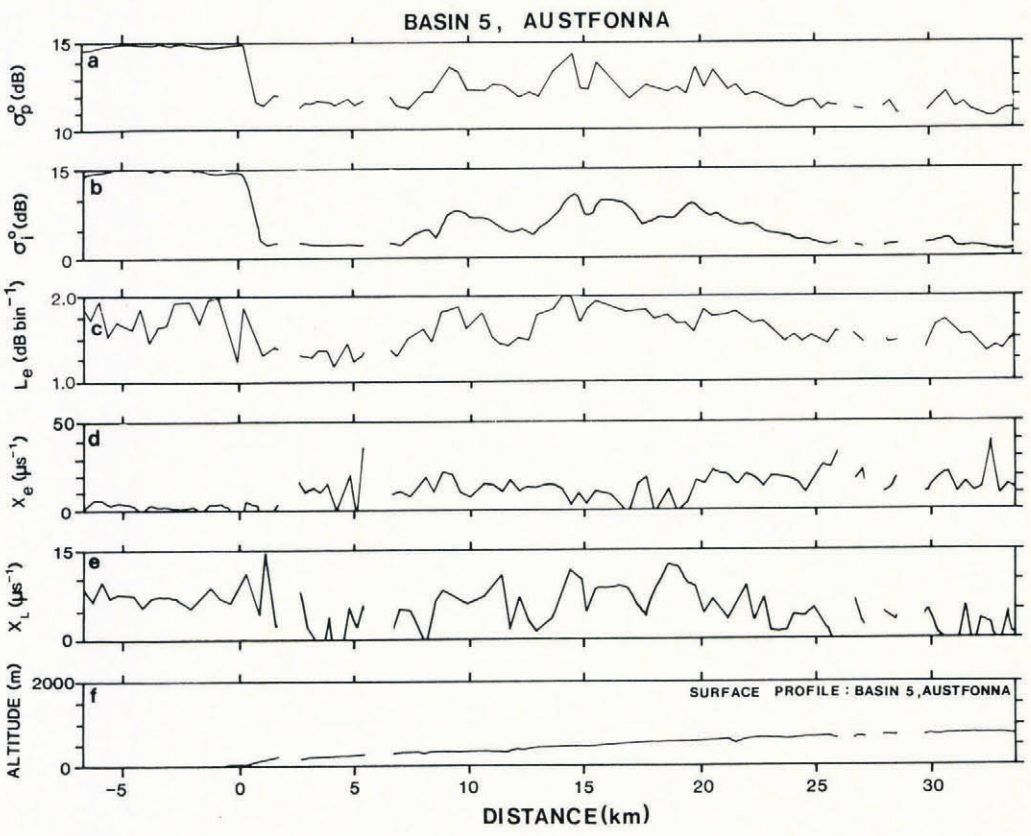

Fig.6. Traces of varying wave-form parameters and ice-surface profile along Basin 5 flight section, Austfonna.

https://doi.org/10.3189/S0260305500200773 Published online by Cambridge University Press

beam-limited footprint. These signals are probably from areas where the snow surface is still relatively dry, and no crevasses have been observed in the upper part of Basin 5. High back-scatter values for drier snow have previously been explained by the effects of a complex snow stratigraphy. Snow layering, ice lamellae, and ice glands or lenses produce a component of specular reflection with typical reflectivity of 0.1, this explaining strong back-scatter limited to near-normal incidence. Snow-pit studies and shallow drilling in Basin 5 during spring 1986 show that such density variations are a common feature of the stratigraphy in this area.

VARIATIONS IN WAVE-FORM PARAMETERS: VESTFONNA

Results

Wave-form parameters from a track across Vestfonna and the central, ice-free valley in Nordaustlandet (Fig.1) indicate three main zones (Fig.7). The first is for the initial 12 km, and is from non-glacierized land. The two values of σ° show several distinct peaks at irregular periods, which are accompanied by rises in L_e of up to 2.0 dB bin^{-1} from a level of around 13 dB bin^{-1}. Both attenuation coefficients are extremely variable, X_e registering a maximum of over 50 μs^{-1} at 6.5 km, but when no signal is evident in late-gate bins X_l returns zeros. Throughout this period spurious delays are recorded, breaks in traces a to f in Fig.7 indicating these occurrences.

The second zone, comprising three short sections, is between approximately 15 and 20 km, 24 and 33 km, and 39 and 42 km. All have the same characteristics with relatively steady values of X_e, at around 20 μs^{-1}. Although back-scatter at nadir (σ°_p) increases by only 1 or 2 dB, σ°_i rises instead by several dB, to plateaus of between 5 and 8 dB. L_e behaves similarly (as at 16 km) by rising by 0.6 dB bin^{-1} to 1.9 dB bin^{-1}.

The final set of short sections last from approximately 20 to 24 km, 33 to 39 km, and from 42 km onwards. σ°_p falls by 1 or 2 dB in places to 12 dB, while σ°_i shows a corresponding decrease to a level of 3 dB. Wave-form leading edges have markedly reduced gradients, with minima at 23 and 35 km of 12 and 11 dB bin^{-1}, respectively. During these periods both trailing-edge coefficients record a large proportion of zeros (Fig.7d and e).

Interpretation

Before crossing the ice streams Bodleybreen, Aldousbreen, and Frazerbreen on Vestfonna, the altimeter traverses Helvetesflya, an area of non-glacierized terrain with several melt lakes. At 1 km, over Flysjøen (the largest lake) signal amplitudes are the highest observed. Although σ°_p only picks out two definite peaks over lakes (at 1 km and 11 km), σ°_i has additional increases at 4 and 5 km. The diffuse nature of signals from Flysjøen, and the TBH of 5°, indicate that the lake surface does not act as a plane reflector, despite minimal metre-scale surface roughness indicated by values for L_e of almost 2.0 dB bin^{-1}. Analysis of Landsat imagery showed that Flysjøen was still ice-covered on 12 July. It is therefore inferred that lake ice, accompanied by surface snow dunes, is a likely cause of the relatively wide polar-scatter diagram and longer-duration returns. Similar wave-form characteristics are observed at 4, 6.5, and 11 km, but at 6.5 km X_e exceeds 50 μs^{-1}. This occurs because mean signals have markedly shorter duration, due to reflection from a more specular surface such as a stream. Otherwise, between the lakes there is a high proportion of spurious delays and rejected wave forms. This, in combination with stretched leading edges, is a response to partially snow-covered terrain having metre-scale roughness of the order of 3 m. Such intermittently snow-covered land was observed on the Landsat scene for 12 July.

The second distinguishable set of areas is beyond about 12 km, where the altimeter begins to traverse Vestfonna. This is the first of several snow-covered and relatively flat ridges with minimal gradient and metre-scale surface roughness (less than 1 m). They return high-amplitude signals. Corresponding 3 dB back-scatter half-angles are approximately 3°.

The last group of areas is associated with ice streams flowing orthogonal to the altimeter flight track and between the series of ridges mentioned above (Fig.7f). They are identifiable both by their distinct surface character and wave-form response. Large-amplitude (15–25 m) kilometre-scale surface roughness has been identified in previous work by Dowdeswell (unpublished), but the L_e minimum of 12 dB

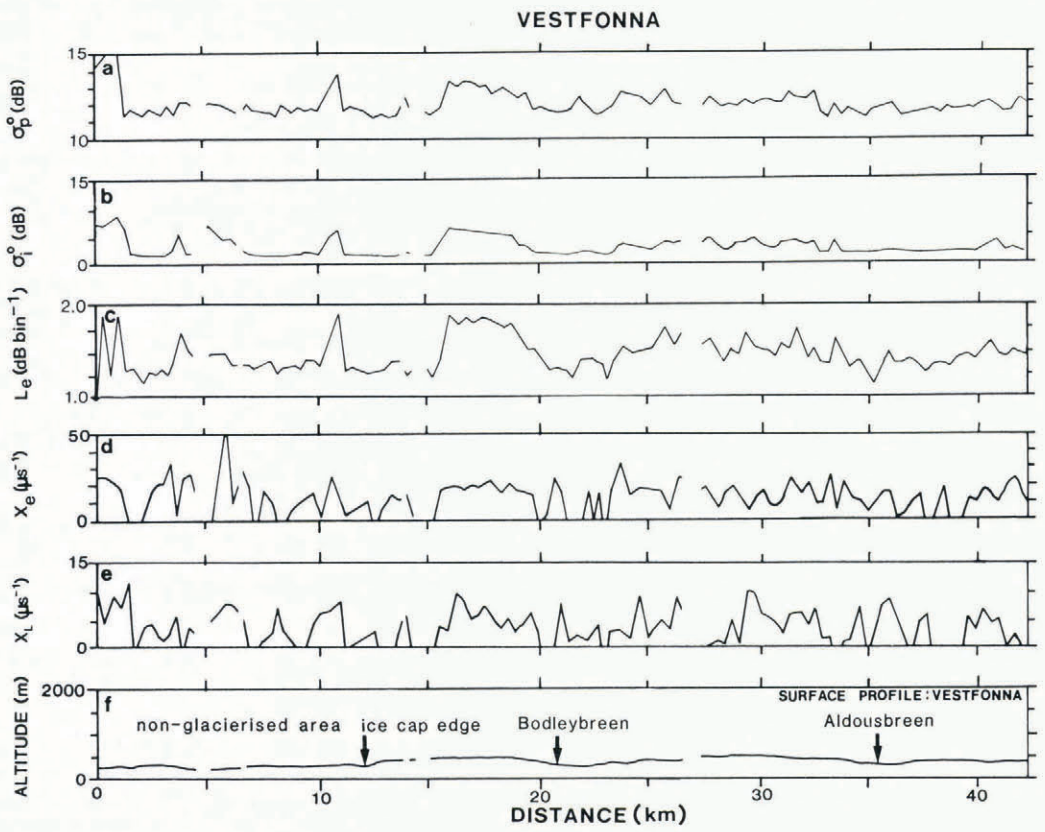

Fig.7. Traces of varying wave-form parameters and ice-surface profile along Vestfonna flight section.

https://doi.org/10.3189/S0260305500200773 Published online by Cambridge University Press

bin^{-1} at 23 km (Fig.7c), for instance, also suggests metre-scale roughness of 3 m or more when compared with predictions for leading-edge gradient made by Brown's model. Bodleybreen (Fig.7f) has surged since 1976 (Dowdeswell 1986). Its boundaries are well defined on Landsat and aerial photographic images of the area by heavy crevassing truncated by shear zones (Fig.3c). The combined roughness and steep lateral margins of Bodleybreen cause severe attenuation of pulses, and loss of the weakest returns. In regions of broken ice the slope distribution is likely to be markedly different than elsewhere and results in TBH of around 5° over parts of Bodleybreen. The other areas of similar wave-form characteristics occur from approximately 33 to 39 km over Aldousbreen, and over the beginning of Frazerbreen from 42 km onwards. Neither has been observed to surge but both are highly crevassed and are faster flowing than the surrounding ridges (Dowdeswell 1986). This surface roughness has a significant effect upon wave forms, in contrast with the signals resulting from surrounding ridges. Small-scale surface roughness is again liable to cause wider scattering and thus the observed longer-duration wave forms.

CONCLUSIONS

Our results indicate that significant variations in returned altimeter signals occur through changes in the terrain type and surface character of Nordaustlandet ice caps. A number of conclusions may be drawn from this work:

1. When wet snow or ice surfaces are encountered Fresnel reflection coefficients are large and a specular component is observed to dominate wave forms.
2. Brown's rough-surface scattering model appears valuable as an indicator of the effects of varying surface character on wave forms.
3. Variations in observed polar scattering suggest that the scattering properties of snow and ice vary across the ice caps. Mean 3 dB back-scatter half-angles of 3° over flat, and relatively less wet snow surfaces correspond with experimental results of Fung and others (1980).
4. Significant changes in surface reflection occur in the early stages of snow surface melt, when free water produced by melting is mainly suspended by necks between snow grains. Previous authors such as Suzuki and others (1983) have noted its importance in influencing the scattering characteristics of the snow surface.
5. Where large-scale surface roughness and crevassing is minimal, as on Bråsvellbreen, differences between the polar-scattering properties of wet and relatively dry snow lead to a significant change in the type of altimetric returns.

Ambiguities remain in the understanding of mechanisms influencing scattering from ice-mass surfaces, and how these in turn affect the general characteristics of mean altimeter wave forms. Further work is needed at 13.6 GHz and at near-nadir into the effects of particular surface properties on radar-altimeter wave forms. This should enable development of algorithms to extract data on key glaciological parameters from the forthcoming generation of satellite radar altimeters (e.g. ERS-1). The delineation of dry and wet snow, and bare-ice zones on large ice masses from altimeter wave-form characteristics should in the future provide valuable information for mass-balance studies.

ACKNOWLEDGEMENTS

We thank Andrew Birks of the Rutherford Appleton Laboratory for providing the Svalbard radar-altimeter data set, and for his assistance with tape handling and back-scatter calibrations. Dr C Rapley and the Algorithm Development Facility, Royal Aircraft Establishment, Farnborough, kindly funded digital image acquisition and processing. Sue Pilkington assisted by drafting the figures. M.R.D. acknowledges support from a UK Natural Environment Research Council studentship. L M Ulander, and Drs N F McIntyre, V A Squire, and G Rees kindly commented on drafts of this paper.

REFERENCES

Brown G S 1977 The average impulse response of a rough surface and its applications. *IEEE Transactions on Antennas and Propagation* AP–25 (1): 67–74

Cumming W A 1952 The dielectric properties of ice and snow at 3.2 centimeters. *Journal of Applied Physics* 23(7): 768–773

Dowdeswell J A 1986 Drainage-basin characteristics of Nordaustlandet ice caps, Svalbard. *Journal of Glaciology* 32(110): 31–38

Dowdeswell J A Unpublished Remote sensing studies of Svalbard glaciers. (PhD thesis, University of Cambridge, 1984)

Dowdeswell J A, McIntyre N F 1986 The saturation of LANDSAT MSS detectors over large ice masses. *International Journal of Remote Sensing* 7(1): 151–164

Dowdeswell J A, Drewry D J, Cooper A P R, Gorman M R, Liestøl O, Orheim O 1986 Digital mapping of the Nordaustlandet ice caps from airborne geophysical investigations. *Annals of Glaciology* 8: 51–58

Evans S 1965 Dielectric properties of ice and snow – a review. *Journal of Glaciology* 5(42): 773–792

Fung A K 1981 A review of surface scatter theories for modeling applications. *In Coherent and incoherent radar scattering from rough surfaces and vegetated areas. Proceedings of an ESA EARSeL Workshop, held at Alpbach, Austria, 16-20 March 1981.* Paris, European Space Agency: 71–82 (ESA SP–166)

Fung A K, Stiles W H, Ulaby F T 1980 Surface effects on the microwave backscatter and emission of snow. *In Institute of Electrical and Electronic Engineers. International Conference on Communications '80. Conference Record* 3: 49.6.1–49.6.7

Gatley C, Peckham G E 1983 *Radar altimetry and scatterometry from aircraft over the oceans.* Edinburgh, Heriot-Watt University. Department of Physics

Gloersen P, Mollo-Christensen E, Wilheit T, Dod T, Kutz R, Campbell W J 1985 *MIZEX '84 NASA CV-990 flight report.* Greenbelt, MD, Goddard Space Flight Center (NASA Technical Memorandum 86216)

Ivanov V B 1968 Eolovyye formy mikrorel'yefa snezhnoy poverkhnosti na lednikakh Antarktidy i Arktiki [Aeolian forms of microrelief of the snow surface of Antarctic and Arctic glaciers]. *Trudy Sovetskoy Antarkticheskoy Ekspeditsii* 38: 22–38

MacArthur J L 1978 *Seasat-A radar altimeter design description.* Baltimore, MD, Johns Hopkins University (Report SDO-5232)

McIntyre N F *and 9 others* 1986 *Analysis of altimetry data from the Marginal Ice Zone Experiment. Final report.* Paris, European Space Agency (Report 5948/84/NL/BI)

Moore R K, Williams C S 1957 Radar terrain return at near-vertical incidence. *Proceedings of the Institute of Radar Engineers* 45: 228–238

Schytt V 1964 Scientific results of the Swedish glaciological expedition to Nordaustlandet, Spitsbergen, 1957 and 1958. *Geografiska Annaler* 46(3): 243–281

Schytt V 1969 Some comments on glacier surges in eastern Svalbard. *Canadian Journal of Earth Sciences* 6(4, Pt 2): 867–873

Smith B M E, Evans S 1972 Radio echo sounding: absorption and scattering by water inclusion and ice lenses. *Journal of Glaciology* 11(61): 133–146

Suzuki M, Matsumoto T, Kuroiwa D, Fujino K, Wakahama G 1983 Research on the interaction of microwaves with snow and ice. Part 1. A study on the microwave backscattering from melting snowpack. *Memoirs of National Institute of Polar Research.* Special Issue 29: 166–175

Ulaby F T, Moore R K, Fung A K 1982 *Microwave remote sensing active and passive. Vol 2. Radar remote sensing and surface scattering and emission theory.* Reading, MA, Addison Wesley

Ulander L Unpublished Airborne radar altimetry over the Greenland ice sheet. (MSc thesis, University of London, 1985)

Zwally H J, Bindschadler R A, Brenner A C, Martin T V, Thomas R H 1983 Surface elevation contours of Greenland and Antarctic ice sheets. *Journal of Geophysical Research* 88(C3): 1589–1596